

Rotation-induced evolution of far-field emission patterns of deformed microdisk cavities

LI GE,^{1,2,*} RAKTIM SARMA,³ AND HUI CAO^{3,4}

¹Department of Engineering Science and Physics, College of Staten Island, CUNY, Staten Island, New York 10314, USA

²The Graduate Center, CUNY, New York, New York 10016, USA

³Department of Applied Physics, Yale University, New Haven, Connecticut 06520-8482, USA

⁴e-mail: hui.cao@yale.edu

*Corresponding author: li.ge@csi.cuny.edu

Received 18 November 2014; revised 23 February 2015; accepted 24 February 2015 (Doc. ID 226931); published 30 March 2015

A critical issue that hinders the development of chip-scale optical gyroscopes is the size dependence of the Sagnac effect, which manifests as a rotation-induced phase shift or frequency splitting between two counter-propagating waves or resonances, and is proportional to the size of the optical system. We show numerically and theoretically that the far-field emission patterns (FFPs) of optical microdisk cavities depend strongly on rotation and can therefore provide an alternative approach. At low rotation speed where resonant frequencies barely shift with rotation (i.e., a negligible Sagnac effect), the FFPs already exhibit a significant rotation-induced asymmetry, which increases linearly with the rotation speed. We further identify the basic requirements to maximize this effect, including distinct output directions for the clockwise and counter-clockwise waves in a cavity mode, as well as a vanishing frequency splitting between one such mode and its symmetry related partner mode. Based on these requirements, we propose several microcavity shapes that display orders of magnitude enhancement of the emission sensitivity to rotation and could stimulate a new generation of optical gyroscopes with small footprints and on-chip integrability. © 2015 Optical Society of America

OCIS codes: (120.5790) Sagnac effect; (000.4430) Numerical approximation and analysis; (060.2800) Gyroscopes; (140.3370) Laser gyroscopes; (140.4780) Optical resonators.

<http://dx.doi.org/10.1364/OPTICA.2.000323>

1. INTRODUCTION

Optical gyroscopes have revolutionized precision measurement of rotation thanks to their scientific ingenuity, affordability, long-term reliability, and compact size [1–5]. They have been widely utilized for both civilian and military aircraft as well as satellites, rockets, and nautical navigation. Meanwhile, optical microcavities have also found a broad range of applications since their debut two decades ago [6,7], from coherent light sources in integrated photonic circuits to cavity quantum electrodynamics, single-photon emitters, and biochemical sensors. Due to their small footprints and on-chip integration

capability, microcavity-based gyroscopes [8–11] can play an important role in reducing the equipment cost in space missions and open the possibility for a new generation of on-chip optical gyroscopes [12].

One obstacle to miniaturization [13–19] is imposed by the current measurement scheme of optical gyroscopes, which is based on the Sagnac effect [1] and has barely changed in the last 50 years since its introduction. The Sagnac effect manifests as a rotation-induced phase shift in a nonresonant structure (e.g., an optical fiber) or a frequency splitting in a resonant cavity, between two counterpropagating waves or resonances;

it is proportional to the size of the cavity, which puts optical microcavities at a serious disadvantage in terms of sensitivity when compared with macroscopic cavities used in current optical gyroscopes. Therefore, to make optical microcavities a viable option for rotation sensing, a new detection scheme must be developed. Previous studies [11,20,21] indicate that the quality (Q) factor of resonant modes also displays a rotation-induced variation, and its relative change can be higher than that of the resonant frequencies. This enhancement, however, is still not sufficient to compensate for the small size of microcavities, with sensitivity far below the Sagnac effect in macroscopic cavities.

In this work we investigate rotation-induced changes of the far-field emission patterns (FFPs) of microdisk resonances. We find a surprisingly strong dependence of FFPs on rotation speed, which may be used as a measurable signature of rotation. This strong FFP sensitivity to rotation is achieved by satisfying three basic requirements. The first one is that the emission is nonisotropic so that the output direction may be changed by rotation. This requirement can be realized by deforming the disk shape from a circle [22–27]. The second requirement is that the clockwise (CW) and counterclockwise (CCW) waves in the nonrotating cavity should have distinct FFPs. Rotation changes the relative weight of CW and CCW waves in a cavity resonance, resulting in a strong change in the FFP when this requirement holds. Finally, the relative weight of CW and CCW waves should be extremely sensitive to rotation even at very low rotation speed. This requirement can be satisfied by minimizing the frequency splitting between a pair of quasi-degenerate resonances in the nonrotating cavity. By implementing these requirements, we show that a dramatic enhancement of the FFP sensitivity to rotation can be achieved.

2. ROTATION-DEPENDENT FAR-FIELD PATTERN

We consider a deformed semiconductor microdisk [22–27] with thickness much less than the radius. Due to the strong index guiding of light in the disk plane, the microdisk can be treated as a two-dimensional (2D) cavity with an effective refractive index n . Here we focus on a cavity with at least one symmetry axis, chosen to be along $\theta = 0, 180^\circ$ in the polar coordinates, and asymmetric cavities will be discussed elsewhere. The disk boundary is described by $\rho(\theta)$, and the symmetry requires $\rho(-\theta) = \rho(\theta)$. When the cavity does not rotate, the resonant modes generally form quasi-degenerate pairs $k_{\text{even}}, k_{\text{odd}}$, whose wave functions have even [$\psi_{\text{even}}(r, \theta) = \psi_{\text{even}}(r, -\theta)$] and odd [$\psi_{\text{odd}}(r, \theta) = -\psi_{\text{odd}}(r, -\theta)$] symmetries about the cavity axis. Therefore, they consist of an equal amount of CW and CCW waves, denoted by $\psi_{m<0}$ and $\psi_{m>0}$, where m is the angular momentum number [see Eq. (2)]. Their FFPs $I_{\text{FFP}}(\theta)$ are both *symmetric* about the symmetry axis, i.e., $I_{\text{FFP}}(-\theta) = I_{\text{FFP}}(\theta)$.

As a microcavity rotates, a pair of such quasi-degenerate $\psi_{\text{even}}, \psi_{\text{odd}}$ resonances couple to each other and gradually become a pair of CW (ψ_{cw}) and CCW (ψ_{ccw}) resonances [8]. The CW and CCW waves experience opposite frequency shifts by rotation, leading to an increase of their frequency splitting

(Sagnac effect). However, such an increase is significant only when the rotation speed exceeds a critical value Ω_c . Below it the frequency splitting barely changes with rotation, which is referred to as a “dead zone” in deformed microcavities [8–10]. However, within the dead zone, the balance between CW and CCW waves in a resonance is already broken by rotation. If the CW and CCW waves have different output directions, the FFP may start changing even within the dead zone. As will be shown in the next section, the unbalance between CW and CCW waves introduces an *asymmetry* in the FFP, which increases *linearly* with rotation speed in the “dead zone” and hence displays a much stronger dependence on rotation speed than the Sagnac effect.

Without loss of generality, we focus on transverse magnetic (TM) resonances whose electric field is perpendicular to the disk plane. We take the angular velocity Ω to be a constant and perpendicular to the cavity plane, with the convention that $\Omega > 0$ indicates a CCW rotation. When $|R\Omega/c| \ll 1$, the resonances of an optical microcavity are determined by the modified Helmholtz equation [8]

$$\left[\nabla^2 + n(\vec{r})^2 \frac{\omega^2}{c^2} + 2i \frac{\omega \Omega}{c} \frac{\partial}{\partial \theta} \right] \psi(\vec{r}) = 0 \quad (1)$$

to the leading order of Ω in the rotating frame. Here R is the average radius of the cavity, $n(\vec{r})$ is the refractive index, ω is the complex resonant frequency of mode $\psi(\vec{r})$, and c is the speed of light in vacuum. To avoid the confusion with the rotation speed, we use the wave vector $k \equiv \omega/c$ instead of ω henceforth. We assume that the detecting apparatus is integrated on the same chip as the microcavity; thus it measures the FFP in the rotating frame where the microcavity is stationary.

To find the optical resonances in a rotating microcavity and their FFPs, one can use the finite-difference time-domain method adapted to the rotating frame [20,28]. Here we employ a frequency-domain method that is grid-free—the scattering matrix method [21]. In this approach the wave function of a resonance is decomposed in the angular momentum basis, i.e., $\psi(\vec{r}) = \sum_{m=0,\pm 1,\pm 2,\dots} A_m(r) e^{im\theta}$, where

$$A_m(r) = \begin{cases} \alpha_m H_m^+(\tilde{k}_m r) + \beta_m H_m^-(\tilde{k}_m r), & r < \rho(\theta), \\ \gamma_m H_m^+(\tilde{k}_m r), & r > \rho(\theta). \end{cases} \quad (2)$$

Here H_m^\pm are the Hankel functions of the first and second kind, describing outgoing and incoming waves. $\tilde{k}_m \equiv [(nk)^2 - 2mk\tilde{\Omega}/R]^{\frac{1}{2}}$ and $\tilde{k}_m \equiv [k^2 - 2mk\tilde{\Omega}/R]^{\frac{1}{2}}$ are m -dependent wave vectors inside and outside the cavity, where $\tilde{\Omega} \equiv R\Omega/c$ is the dimensionless rotation speed.

A. Case Study: Symmetric Limaçon Cavity

The first example we analyze is the limaçon cavity, whose boundary is given by $\rho(\theta) = R(1 + \varepsilon \cos \theta)$, where ε is the deformation parameter. Over a wide range of ε , the cavity supports resonances with high Q -factor and directional emission [24]. Figure 1(a) shows a ψ_{even} resonance at $\varepsilon = 0.41$. This whispering-gallery (WG) like resonance has the normalized frequency $k_{\text{even}} R \simeq 33.78$, which has dominant angular

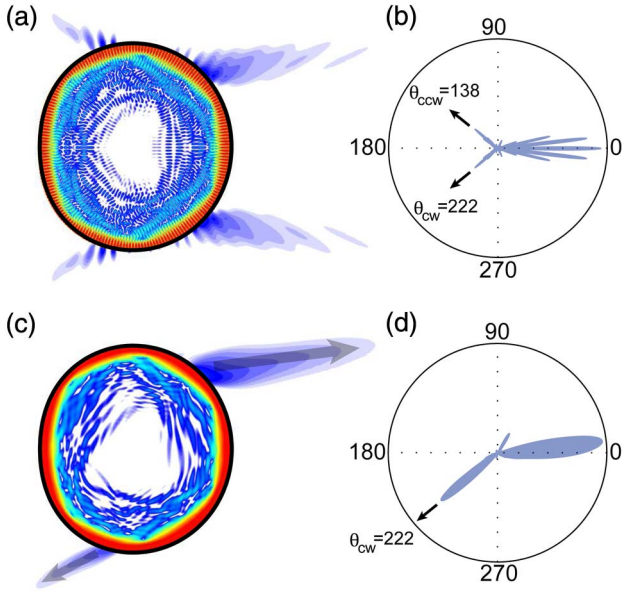


Fig. 1. Near-field and far-field intensity patterns of a nonrotating limaçon cavity. (a) Near-field intensity pattern in the logarithmic scale and (b) far-field intensity pattern in the polar coordinates of a symmetric resonance ψ_{even} at $k_{\text{even}}R \approx 33.78$. The cavity deformation is $\varepsilon = 0.41$, and the refractive index is $n = 3$. The resonance is concentrated near the cavity boundary, similar to a whispering-galley mode. Its emission is directional, with the main direction centered in $\theta = 0^\circ$ and the secondary peaks in $\theta \approx 138^\circ$ and $-138^\circ = 222^\circ$. The CW wave component of this resonance is separated and plotted in (c) and (d). Its mirror image about the horizontal axis gives the CCW wave (not shown).

components $m = \pm 101$ and corresponds to a vacuum wavelength $\lambda \approx 930$ nm if we take $R = 5$ μm . The FFP in Fig. 1(b) shows that the emission is predominantly in the forward direction $\theta = 0$.

As mentioned previously, the cavity symmetry $\rho(\theta) = \rho(-\theta)$ determines that the CW and CCW waves in its resonances at rest have the same magnitude. The CW wave of this ψ_{even} resonance has two main peaks in the FFP, one near $\theta = 0$ and a slightly weaker one at $\theta_{\text{cw}} \approx -138^\circ = 222^\circ$ [Fig. 1(d)]; they are attributed to the chaotic diffusion of optical rays inside the cavity [24,29], which can be seen in the logarithmic-scale intensity plot in Fig. 1(c). The mirror image of these patterns about the symmetry axis gives the FFP of the CCW wave, with the secondary peak located at $\theta_{\text{ccw}} \approx 138^\circ$. The constructive interference of the CW and CCW waves enhances the emission near $\theta = 0$ of the ψ_{even} resonance.

As the cavity rotates, the initial balance between the amplitudes of the CW and CCW waves is broken, which is similar to the finding in closed billiards [8]. In this ψ_{even} resonance the CW wave becomes stronger with rotation speed, and the intensity peak at θ_{cw} increases with respect to the ones at θ_{ccw} and $\theta = 0$ [see Fig. 2(a)], leading to an *asymmetric* FFP. The opposite takes place in the corresponding odd-symmetry resonance ψ_{odd} , with the CCW wave becoming prevailing and an increasing intensity peak at θ_{ccw} (not shown). Consequently, we find that the CW and CCW waves ($\psi_{m<0}$, $\psi_{m>0}$) in the ψ_{even} , ψ_{odd} resonances at rest give good approximations of the

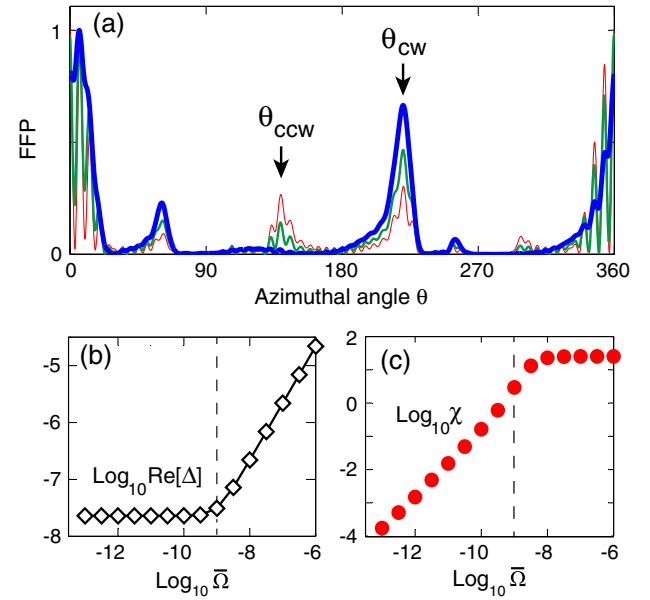


Fig. 2. Rotation-induced changes in resonance frequency and far-field emission pattern of a limaçon cavity. (a) Far-field intensity pattern of the resonance shown in Fig. 1 when the dimensionless rotation speed $\bar{\Omega} = 10^{-8}$ (thick line), 10^{-9} (medium line), and 10^{-10} (thin line). The maximum intensity is normalized to 1 for each curve. Rotation enhances the emission peak at θ_{cw} and reduces the one at θ_{ccw} . (b) Dimensionless frequency splitting Δ of the quasi-degenerate resonances as a function of the normalized rotation speed $\bar{\Omega}$. Δ remains nearly constant below $\bar{\Omega}_c \approx 10^{-9}$ (marked by the vertical dashed line), marking a “dead zone” for the Sagnac effect. The diamonds represent the numerical data, and the solid line shows the result of the coupled-mode theory, Eq. (4). (c) Rotation-induced FFP asymmetry χ as a function of $\bar{\Omega}$. χ increases linearly with $\bar{\Omega}$ inside the “dead zone.”

CW and CCW resonances (ψ_{cw} , ψ_{ccw}) at high rotating speed, i.e., $\psi_{\text{cw}} \approx \psi_{m<0}$ and $\psi_{\text{ccw}} \approx \psi_{m>0}$.

For the FFP evolution to have a strong dependence on rotation, obviously we require ψ_{cw} , ψ_{ccw} to have very different FFPs from ψ_{even} , ψ_{odd} . It is clear from the discussion above that this criterion can be directly evaluated in a cavity at rest, by requiring that $\psi_{m<0}$ and $\psi_{m>0}$ have very different FFPs. In a limaçon cavity the FFP peaks of $\psi_{m<0}$ at θ_{cw} and $\psi_{m>0}$ at θ_{ccw} satisfy this requirement. Utilizing this difference, the evolution of the FFP $I_{\text{FFP}}(\theta)$ of the ψ_{even} resonance shown in Fig. 2(a) can be quantified by the asymmetry

$$\chi(\bar{\Omega}) = \frac{\int_{\theta_{\text{cw}}-\sigma/2}^{\theta_{\text{cw}}+\sigma/2} I_{\text{FFP}}(\theta; \bar{\Omega}) d\theta}{\int_{\theta_{\text{ccw}}-\sigma/2}^{\theta_{\text{ccw}}+\sigma/2} I_{\text{FFP}}(\theta; \bar{\Omega}) d\theta} - 1, \quad (3)$$

where σ is the angular detection window of each peak and taken to be 15° . We note $\chi(\bar{\Omega} = 0) = 0$.

In Figs. 2(b) and 2(c) we show how the Sagnac effect, given by the real part of the dimensionless frequency splitting $\Delta = [k_{\text{cw}} - k_{\text{ccw}}]R$ of the ψ_{cw} , ψ_{ccw} resonances, and the FFP asymmetry χ evolve with rotation speed. The “dead zone” for Δ lies below a critical speed $\bar{\Omega}_c \sim 10^{-9}$ (or equivalently, $\Omega \sim 6 \times 10^4$ rad/s), within which Δ barely changes. In

contrast, χ displays a linear increase with the rotation speed $\bar{\Omega}$ in the “dead zone,” based on which the rotation speed can be detected. The minimum detectable $\bar{\Omega}$ scales linearly with the smallest asymmetry that can be detected in the FFP measurement. For example, if we assume that $\min[\chi] \sim 10^{-4}$, the lowest rotation speed that can be measured is $\bar{\Omega} \approx 10^{-13}$, or equivalently, $\bar{\Omega} \sim 6$ rad/s. This performance is comparable to commercial optical gyroscopes based on the Sagnac effect in macrocavities, whose sensitivity would be 10^4 times lower when simply scaled down to microcavities.

B. Further Enhancement of Far-Field Sensitivity to Rotation

To enhance the FFP sensitivity to rotation, we conduct a quantitative analysis with the coupled-mode theory. The increase of the FFP asymmetry χ with the rotation speed can be attributed to the mixing of one resonance with others by rotation. Since ψ_{even} and ψ_{odd} are quasi-degenerate, their mutual coupling is much stronger than the coupling with other resonances farther away in frequency [30,31]. Therefore, we can approximate $\psi(\bar{\Omega}) \approx a_{\text{even}}(\bar{\Omega})\psi_{\text{even}} + a_{\text{odd}}(\bar{\Omega})\psi_{\text{odd}}$ [8–10,21], which gives the frequency splitting

$$\Delta(\bar{\Omega}) \approx [\Delta_0^2 + g^2\bar{\Omega}^2]^{\frac{1}{2}}. \quad (4)$$

Here $\Delta_0 \equiv \Delta(\bar{\Omega} = 0)$ and g is the dimensionless coupling constant between ψ_{even} and ψ_{odd} , which are approximately real for high- Q resonances [21]. In a deformed microcavity, $\Delta_0 \neq 0$ in general, and the dead zone is determined by $\bar{\Omega}_c \equiv |\Delta_0|/g$. When $\bar{\Omega} \gg \bar{\Omega}_c$, Δ approaches its asymptote $\Delta(\bar{\Omega}) \approx g\bar{\Omega}$ and displays the familiar linear scaling of the Sagnac effect. Below $\bar{\Omega}_c$, the rotation-induced splitting ($g\bar{\Omega}$) is much smaller than the intrinsic splitting (Δ_0), and the Sagnac effect becomes very weak as shown in the “dead zone” in Fig. 2(b). Using $g = 21.45 - 0.004i$ and $\Delta_0 = (2.29 + 0.90i) \times 10^{-8}$ from the scattering matrix calculation, Eq. (4) gives a good approximation of $\bar{\Omega}_c \approx 1.07 \times 10^{-9}$.

A high rotation sensitivity of the FFP asymmetry requires a rapid increase of the mixing ratio $\xi(\bar{\Omega}) \equiv a_{\text{odd}}(\bar{\Omega})/a_{\text{even}}(\bar{\Omega})$ with rotation speed, in addition to very different FFPs for $\psi_{m<0}$ and $\psi_{m>0}$ at rest. Deep in the dead zone ($\bar{\Omega} \ll \bar{\Omega}_c$), the mixing ratio $\xi(\bar{\Omega})$ in the initially ψ_{even} resonance is approximately

$$\xi(\bar{\Omega}) \approx \pm i \frac{\bar{\Omega}}{2\Omega_c}, \quad (5)$$

from which we see immediately that the key quantity is a small $\bar{\Omega}_c$, or equivalently, a small frequency splitting Δ_0 at rest and a large coupling g between ψ_{even} , ψ_{odd} resonances. g is proportional to the optical path length and hence limited by the small size of microcavities. Δ_0 , however, can be reduced by using microcavities with more than one symmetry axis [9].

One example is the microcavity with spatial symmetry described by the dihedral group D_3 , $\rho(\theta) = R(1 + \epsilon \cos 3\theta)$ [9], which we will simply refer to as the D_3 cavity (see Fig. 3). Ideally Δ_0 can be entirely eliminated for the resonances

whose angular momenta m in Eq. (2) are not integer multiples of 3, giving a linear increase of the frequency splitting Δ with the rotation speed $\bar{\Omega}$ [Fig. 3(d)]. In practice, there is always inherent surface roughness introduced unintentionally during the fabrication process, which breaks the exact D_3 symmetry and lifts the degeneracy of ψ_{even} , ψ_{odd} at rest slightly. Thus a “dead zone” is created, but its size is expected to be much smaller than the intrinsic one, e.g., for the limaçon cavity. The resulting small $\bar{\Omega}_c$ greatly enhances the rotation dependence of the FFP asymmetry at low speed, given that the $\psi_{m<0}$ and $\psi_{m>0}$ waves also have very different FFPs here [Fig. 3(b)]. To visualize this expected enhancement, we plot χ by constructing $\psi(\bar{\Omega}) \propto \psi_{\text{even}} + \xi(\bar{\Omega})\psi_{\text{odd}}$; ψ_{even} , ψ_{odd} are directly obtained by the scattering matrix method, and $\xi(\bar{\Omega})$ can be

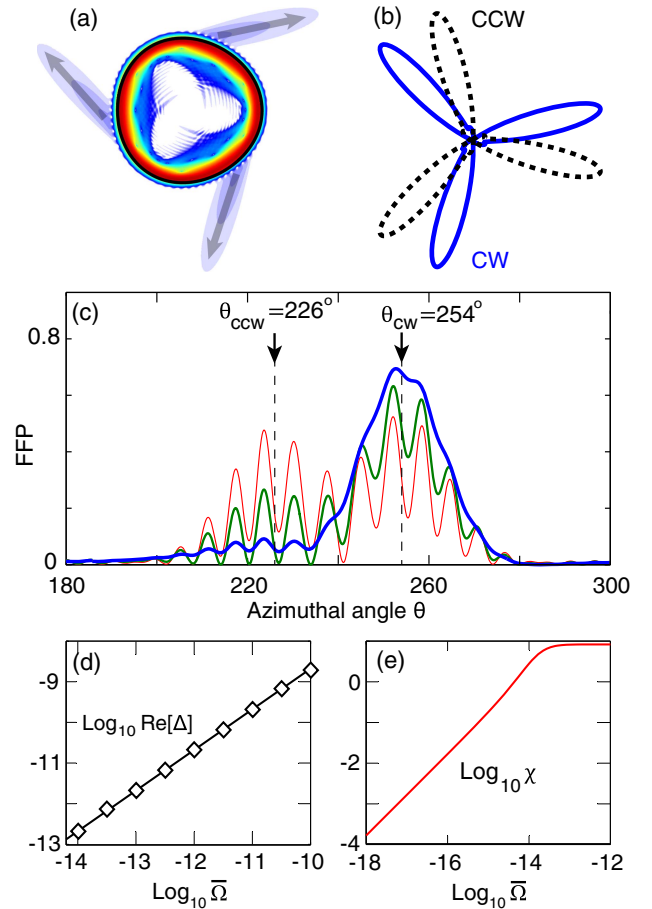


Fig. 3. Enhanced sensitivity of far-field emission pattern to rotation in a D_3 cavity with $R = 5 \mu\text{m}$ and $n = 3$. (a) Near-field intensity plot of the CW wave in a whispering-gallery-like resonance at $k_{\text{even}}R \approx 33.80$ in the logarithmic scale. The dominant angular components of this resonance are $m = \pm 94$. (b) Distinct FFPs in the polar coordinates of CW (solid) and CCW (dotted) waves at rest. (c) Far-field intensity pattern at $\bar{\Omega} = 10^{-13}$ (thick line), 10^{-14} (medium line), and 10^{-15} (thin line). (d) Dimensionless frequency splitting Δ as a function of the normalized rotation speed $\bar{\Omega}$, showing a linear increase due to the vanishing “dead zone”. The diamonds represent the numerical data, and the solid line shows the result of the coupled-mode theory, Eq. (4). (e) Rotation-induced FFP asymmetry χ of the ψ_{even} resonance as a function of $\bar{\Omega}$. $\theta_{\text{cw}} = 254^\circ$, $\theta_{\text{ccw}} = 226^\circ$ (equivalent to the one at -254°), and $\sigma = 15^\circ$ are used in calculating $\chi(\bar{\Omega})$ from Eq. (3).

calculated from Eq. (5), using $g \approx 20.62$ again from the scattering matrix method and taking $\Omega_c = 10^{-14}$, which is 10^5 smaller than that in the limaçon case. The result is shown in Figs. 3(c) and 3(e), and a rotation sensitivity of χ is enhanced by roughly the same factor, i.e., 10^5 , at low speed when compared with the limaçon cavity shown in Fig. 2(b): now $\chi = 10^{-4}$ corresponds to $\tilde{\Omega} \approx 10^{-18}$ instead of 10^{-13} .

3. DISCUSSION AND CONCLUSION

In summary, we have investigated how rotation modifies the FFPs of open microcavities. In a 2D cavity deformed from a circle and with at least one symmetry axis, the FFPs are non-isotropic and each resonance has equal CW and CCW wave components at rest. Rotation breaks the balance between CW and CCW waves, causing a significant change in the FFP, if the CW and CCW waves have distinct output directions. At low rotation speed where the resonant frequencies barely shift with rotation, the FFPs already exhibit asymmetry, which increases linearly with the rotation speed. The sensitivity of the FFPs to rotation can be enhanced by reducing the intrinsic splitting $\Delta\Omega_0$ of quasi-degenerate resonances at rest, achievable via engineering the cavity shape. For example, the D_3 symmetry can support degenerate resonances with directional emission. Using a perturbation theory [30–32], one can show that the small $\Delta\Omega_0$ in a D_3 cavity due to surface roughness scales inversely with the system size to the leading order, and hence a larger cavity will have a stronger sensitivity to rotation. To eliminate this residual $\Delta\Omega_0$, one solution is using the hexagonal cavity, which also possesses the D_3 symmetry and supports degenerate resonances. Since single-crystalline GaN or ZnO disks with hexagonal cross section can be grown with atomic flat surfaces [33–36], $\Delta\Omega_0$ due to surface roughness can be greatly reduced. Finally we comment that the current study is focused on the FFP change of individual resonances in the linear regime. It would be interesting to explore the simultaneous excitation of multiple resonances and their nonlinear interactions in rotating microcavities in future work.

FUNDING INFORMATION

National Science Foundation (NSF) (DMR-1205307); Office of Naval Research (ONR) (MURI SP0001135605); Research Foundation of The City University of New York (RFCUNY) (PSC-CUNY 45).

ACKNOWLEDGMENT

We thank Takahisa Harayama and Jan Wiersig for helpful discussions. L. G. acknowledges the PSC-CUNY 45 Research Grant and the Provost Research Fellowship by the College of Staten Island. R. S. and H. C. acknowledge NSF support under grant nos. DMR-1205307 and ONR MURI SP0001135605.

REFERENCES

1. E. J. Post, "Sagnac effect," *Rev. Mod. Phys.* **39**, 475–493 (1967).
2. W. W. Chow, J. Gea-Banacloche, L. M. Pedrotti, V. E. Sanders, W. Schleich, and M. O. Scully, "The ring laser gyro," *Rev. Mod. Phys.* **57**, 61–104 (1985).
3. F. Aronowitz, "The laser gyro," in *Laser Applications* (Academic, 1971), pp. 113–200.
4. C. Ciminelli, F. Dell'Olio, C. E. Campanella, and M. N. Armenise, "Photonic technologies for angular velocity sensing," *Adv. Opt. Photon.* **2**, 370–404 (2010).
5. M. Terrel, M. J. F. Digonnet, and S. Fan, "Performance comparison of slow-light coupled-resonator optical gyroscopes," *Laser Photon. Rev.* **3**, 452–465 (2009).
6. R. K. Chang and A. J. Campillo, eds., *Optical Processes in Microcavities*, Advanced Series in Applied Physics (World Scientific, 1996).
7. K. J. Vahala, ed., *Optical Microcavities*, Advanced Series in Applied Physics (World Scientific, 2004).
8. S. Sunada and T. Harayama, "Sagnac effect in resonant microcavities," *Phys. Rev. A* **74**, 021801(R) (2006).
9. S. Sunada and T. Harayama, "Design of resonant microcavities: application to optical gyroscopes," *Opt. Express* **15**, 16245–16254 (2007).
10. S. Sunada, S. Tamura, K. Inagaki, and T. Harayama, "Ring-laser gyroscope without the lock-in phenomenon," *Phys. Rev. A* **78**, 053822 (2008).
11. J. Scheuer, "Direct rotation-induced intensity modulation in circular Bragg micro-lasers," *Opt. Express* **15**, 15053–15059 (2007).
12. <http://www.mermig-space.eu/>, accessed 2/22/15.
13. A. B. Matsko, A. A. Savchenkov, V. S. Ilchenko, and L. Maleki, "Optical gyroscope with whispering gallery mode optical cavities," *Opt. Commun.* **233**, 107–112 (2004).
14. B. Z. Steinberg, "Rotating photonic crystals: a medium for compact optical gyroscopes," *Phys. Rev. E* **71**, 056621 (2005).
15. J. Scheuer and A. Yariv, "Sagnac effect in coupled-resonator slow-light waveguide structures," *Phys. Rev. Lett.* **96**, 053901 (2006).
16. B. Z. Steinberg, J. Scheuer, and A. Boag, "Rotation-induced superstructure in slow-light waveguides with mode-degeneracy: optical gyroscopes with exponential sensitivity," *J. Opt. Soc. Am. B* **24**, 1216–1224 (2007).
17. C. Peng, Z. Li, and A. Xu, "Optical gyroscope based on a coupled resonator with the all-optical analogous property of electromagnetically induced transparency," *Opt. Express* **15**, 3864–3875 (2007).
18. C. Sorrentino, J. R. E. Toland, and C. P. Search, "Ultra-sensitive chip scale Sagnac gyroscope based on periodically modulated coupling of a coupled resonator optical waveguide," *Opt. Express* **20**, 354–363 (2012).
19. R. Novitski, B. Z. Steinberg, and J. Scheuer, "Losses in rotating degenerate cavities and a coupled-resonator optical-waveguide rotation sensor," *Phys. Rev. A* **85**, 023813 (2012).
20. R. Sarma and H. Cao, "Wavelength-scale microdisks as optical gyroscopes: a finite-difference time-domain simulation study," *J. Opt. Soc. Am. B* **29**, 1648–1654 (2012).
21. L. Ge, R. Sarma, and H. Cao, "Rotation-induced asymmetry of far-field emission from optical microcavities," *Phys. Rev. A* **90**, 013809 (2014).
22. J. U. Nöckel and A. D. Stone, "Ray and wave chaos in asymmetric resonant optical cavities," *Nature* **385**, 45–47 (1997).
23. C. Gmachl, F. Capasso, E. E. Narimanov, J. U. Nöckel, A. D. Stone, J. Faist, D. L. Sivco, and A. Y. Cho, "High-power directional emission from microlasers with chaotic resonators," *Science* **280**, 1556–1564 (1998).
24. J. Wiersig and M. Hentschel, "Combining directional light output and ultralow loss in deformed microdisks," *Phys. Rev. Lett.* **100**, 033901 (2008).
25. Q. Song, L. Ge, A. D. Stone, H. Cao, J. Wiersig, J.-B. Shim, J. Unterhinninghofen, W. Fang, and G. S. Solomon, "Directional laser emission from a wavelength-scale chaotic microcavity," *Phys. Rev. Lett.* **105**, 103902 (2010).
26. B. Redding, L. Ge, Q. H. Song, J. Wiersig, G. S. Solomon, and H. Cao, "Local chirality of optical resonances in ultrascale resonators," *Phys. Rev. Lett.* **108**, 253902 (2012).

27. B. Redding, L. Ge, Q. H. Song, G. S. Solomon, and H. Cao, "Manipulation of high-order scattering processes in ultrasmall optical resonators to control far-field emission," *Phys. Rev. Lett.* **112**, 163902 (2014).
28. R. Novitski, J. Scheuer, and B. Z. Steinberg, "Unconditionally stable finite-difference time-domain methods for modeling the Sagnac effect," *Phys. Rev. E* **87**, 023303 (2013).
29. H. G. Schwefel, N. B. Rex, H. E. Türeci, R. K. Chang, A. D. Stone, T. Ben-Messaoud, and J. Zyss, "Dramatic shape sensitivity of directional emission patterns from similarly deformed cylindrical polymer lasers," *J. Opt. Soc. Am. B* **21**, 923–934 (2004).
30. L. Ge, Q. H. Song, B. Redding, and H. Cao, "Extreme output sensitivity to subwavelength boundary deformation in microcavities," *Phys. Rev. A* **87**, 023833 (2013).
31. L. Ge, Q. Song, B. Redding, A. Eberspächer, J. Wiersig, and H. Cao, "Controlling multimode coupling by boundary-wave scattering," *Phys. Rev. A* **88**, 043801 (2013).
32. R. Dubertrand, E. Bogomolny, N. Djellali, M. Lebental, and C. Schmit, "Circular dielectric cavity and its deformations," *Phys. Rev. A* **77**, 013804 (2008).
33. K. Hiramatsu, K. Nishiyama, M. Onishi, H. Mizutani, M. Narukawa, A. Motogaito, H. Miyake, Y. Iyechika, and T. Maeda, "Fabrication and characterization of low defect density GaN using facet-controlled epitaxial lateral overgrowth (FACELO)," *J. Cryst. Growth* **221**, 316–326 (2000).
34. C. Kim, Y.-J. Kim, E.-S. Jang, G.-C. Yi, and H. H. Kim, "Whispering-gallery-modelike-enhanced emission from ZnO nanodisk," *Appl. Phys. Lett.* **88**, 093104 (2006).
35. D. J. Gargas, M. C. Moore, A. Ni, S.-W. Chang, Z. Y. Zhang, S.-L. Chuang, and P. D. Yang, "Whispering gallery mode lasing from zinc oxide hexagonal nanodisks," *ACS Nano* **4**, 3270–3276 (2010).
36. C. Tessarek, G. Sarau, M. Kiometzis, and S. Christiansen, "High quality factor whispering gallery modes from self-assembled hexagonal GaN rods grown by metal-organic vapor phase epitaxy," *Opt. Express* **21**, 2733–2740 (2013).